Deformable B-Solids and Implicit Snakes for Localization and Tracking of SPAMM MRI-Data

Petia Radeva, Amir Amini*,†, Jiantao Huang† and Enric Martí
CVC, Departament d'Informatica,
Universitat Autonoma de Barcelona, 08193 Bellaterra (Barcelona), SPAIN
petia,enric@upisun1.uab.es

Departments of †Electrical Engineering and *Diagnostic Radiology,
Yale University, New Haven, CT 06520, USA
e-mail: amini,wangjz@minerva.cis.yale.edu

Abstract

To date, MRI-SPAMM data from different image slices have been analyzed independently. In this paper, we propose an approach for 3D tag localization and tracking of SPAMM data by a novel deformable B-solid. The solid is defined in terms of a 3D tensor product B-spline. The iso-parametric curves of the B-spline solid have special importance. These are termed implicit snakes as they deform under image forces from tag lines in different image slices. The localization and tracking of tag lines is performed under constraints of continuity and smoothness of the B-solid. The framework unifies the problems of localization, and displacement fitting and interpolation into the same procedure utilizing B-spline bases for interpolation. To track motion from boundaries and restrict image forces to the myocardium, a volumetric model is employed as a pair of coupled endocardial and epicardial B-spline surfaces. To recover deformations in the LV an energy-minimization problem is posed where both tag and LV boundary data are used. The framework has been implemented on tag data from Short Axis (SA) cardiac images, as well as SA left ventricle (LV) boundaries, and is currently being extended to include Long Axis (LA) data.

1. Introduction

Tagged MRI is an excellent technique for measuring non-rigid tissue motion. SPAMM[3] produces a grid pattern of signal voids on the tissue - two perpendicular sets of tag planes, each perpendicular to the imaging planes (see Fig. 5). The resulting pattern defines a time-varying curvilinear coordinate system on the tissue.

Accurate detection of tags is crucial to measurement of deformations and understanding of myocardial function. In [2, 6, 9] detection of tag stripes is performed by graph search and tag profile fitting. In order to determine the tag locations, tag profiles are simulated as a function of time using physics of MRI. The profile fitting approach has been improved by utilizing a template matching procedure in [1, 2]. In [1, 10, 18], authors have adopted a 2D snake technique for different image slices to recover within slice tag motion. Their approach aims to minimize an external energy which is the sum of intensities for each slice, together with an internal energy which provides smoothness. As pointed out in [10], detection of tag data with varying contrast needs spatially varying parameters for snakes, making automated localization non-trivial.

Our goal in this work is to develop a model for detection of local deformations of the LV based on tag and contour data. We extend to 3D the previous approach of detecting locally deforming tag stripes using 2D deformable grids [1, 2, 18]. We employ a planar surface description for the tag planes in the form of deformable iso-parametric surfaces of a B-solid, and provide the necessary smoothness constraints required in robust localization of tag information. Such an extension is justified by the fact that different slices represent parts of the same continuous body. In particular, tag lines appearing in different slices belong to continuous tag planes and thus should satisfy across and within slice smoothness constraints. For this purpose tag lines in different slices are detected by a set of implicit snakes that are part of the B-solid model. As an additional point, inhomogeneities in T_1 of myocardial tissue leads to different tag points being visible up to different times. Propagation of information across slices helps with such data analysis issues.

The B-solid is implemented as a 3D tensor product B-

spline model. This is a compact model, yet it is flexible enough to follow the movement of the LV with high accuracy. Its compactness results from the B-solid being completely defined by a set of control points much smaller in number than the number of voxels in the volume. In the deformable B-solid, two sets of iso-parametric surfaces are aligned with parallel lines of tag grids from the sequence of SA images. A set of twice iso-parametric curves links the tag intersections from different slices. We refer to the curves which are formed from intersection of iso-parametric surfaces with image slices as implicit snakes. Implicit snakes are attracted to tag data and deform the B-solid.

Detection and estimation of three-dimensional local tag deformation were previously considered as two separate procedures [12, 13, 18]. Usually, the second step corresponds to constructing a volumetric heart model using information from tags and contours. All of these perform a global fit with the heart contours and deform in accordance with the tag data displacements. In the B-solid approach, as a byproduct of representing the tags by implicit snakes, localization and displacement fitting and interpolation of tag information are performed in a single procedure (interpolation is performed with B-spline bases). Appropriate external forces of the B-solid attract these curves to tag data, adjusting the B-solid, and hence tracking the local deformation of the tissue. In this paper, we consider only SA image slices, and as such consider external forces from the image planes which alter the position of the implicit snakes within image slices. Though external forces thus far come from image slices, internal forces are applied in 3D to the B-solid.

A common feature of most heart motion reconstruction schemes is that they only use tag intersections [13, 18] or intersections between tags and myocardial contours to detect the local deformation of the heart tissue. Analysis with such sparse tag data neglect valuable information contained at other locations along tag lines [2]. The B-solid also uses all the information contained in tag displacements. Furthermore, the B-solid has no parameters to adjust except the parameters of elasticity of the implicit snakes.

Improvements are also proposed here, for snake analysis of tag data. In particular, the usual internal forces are modified to preserve characteristics of an ideal B-solid. As a consequence, the shrinking problem of the snakes is bypassed. To provide a contrast-independent detector for dark tag bands, we construct directional potential fields from principal curvature features of tagged images. The directional sensitivity of the potentials has the advantage that implicit snakes are attracted only by tag lines with similar orientations.

In addition to the deformable B-solid, we consider a B-spline representation for the LV boundaries [8] attached to the B-solid. The deformable B-spline LV model possesses local control, allowing the representation to better adjust to the data and interpolate the contours providing an accurate representation for the heart. In contrast, most of the available models [13, 18] are designed to perform a global fit to the heart contours, and hence can at best roughly approximate the contours.

The rest of the paper is organized as follows: section 2 introduces the deformable B-solid, section 3 discusses energies associated with the B-solid, sections 4 and 5 define the localization by the B-solid and heart model, and section 6 considers the tracking problem for the B-solid. In section 7 an extension of the B-solid approach to SA and LA images analysis is outlined and finally, conclusions are given.

2. Deformable B-Solid

In this section, we discuss implicit snakes and the B-solid. As will be described, implicit snakes track the deformations resulting from the tag data. A heart model will be described which is designed to track the endocardial and epicardial boundaries, and is attached to the B-solid. The use of two models is necessary to achieve high precision in representing both tag and contour structures.

2.1. Definition of Deformable B-Solid

We define the B-solid as a 3D tensor product B-spline with iso-parametric surfaces corresponding to the tagging and imaging planes (see Fig. 1). The B-solid has all the attractive properties of B-splines: (1) B-splines provide local control of shape, allowing for exactly fitting the deformed tag planes. In addition, individual movement of control points only affect the solid's shape locally. (2) Cubic B-splines possess second order continuity everywhere. Moreover, due to parametric continuity, representing tag lines with B-splines allows for sub-pixel localization of tag features. (3) The degree of blending polynomials is independent of the number of control points, and furthermore the solid is completely specified by few control points.

We define the B-solid as a 3D tensor product B-spline,

$$Q(u,v,w) = \sum_{i=0}^{I}\sum_{j=0}^{J}\sum_{k=0}^{K} S_{kji} B_i(u) B_j(v) B_k(w),$$

where $B_i(u),\ B_j(v)$ and $B_k(w)$ are the B-spline blending functions and $S_{kji}, k = 0, \ldots K, j = 0, \ldots J, i = 0, \ldots I$, are the control points of the B-solid. Cubic B-splines have an optimal approximation property, namely, that among all interpolants they minimize the norm of the second derivative. As we will consider thin-plate energy of the B-solid in our energy-based formulation, it is also reasonable to construct the deformable model with a cubic degree.

In a SA acquisition, the u and v iso-parametric surfaces are aligned with tag planes, and the $u - v$ iso-parametric

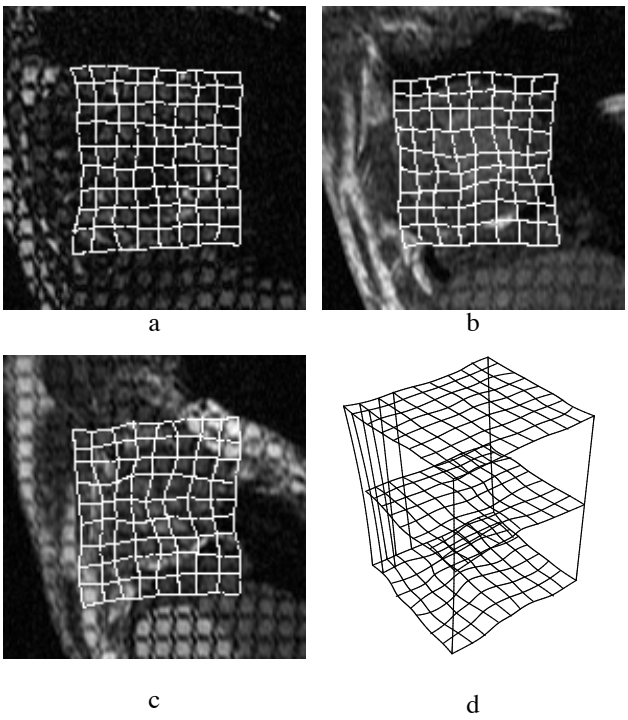

Figure 1. Tag grids detected by implicit snakes of the B-solid on different image slices (a,b,c) determine a B-solid (d)

curves link tag intersections from different slices (see Fig. 1 and Fig. 2). Thus, u and v iso-parametric planes deform with tag planes and w - with SA imaging planes.

2.2. Heart Model

Given the epicardial and endocardial surfaces of the heart, we can represent this information as a pair of coupled boundary surfaces of the endocardium and epicardium using tensor product B-splines:

$$H(x,y,z) = \sum_{o=0}^{O}\sum_{p=0}^{P}\sum_{q=0}^{Q} H_{qpo} B_o(\overline{u}) B_p(\overline{v}) B_q(\overline{w})$$

where H_{qpo} are the control points and $(\overline{u},\overline{v},\overline{w})$ are the coordinates of the LV model. The $\overline{u}$ iso-parametric curves coincide with the inner and outer contours from each slice and, due to the closed curves, the corresponding blending functions are periodic. The $\overline{v}$-iso-parametric curves link the epicardial and endocardial contour from each slice, and the $\overline{w}$-iso-parametric curves go through the contours from the different slices (see Fig. 2). Their corresponding classes of blending functions are non-periodic. To consider the complete shape from apex to base, we place multiple knots at apex, hence creating the oval shape of the LV.

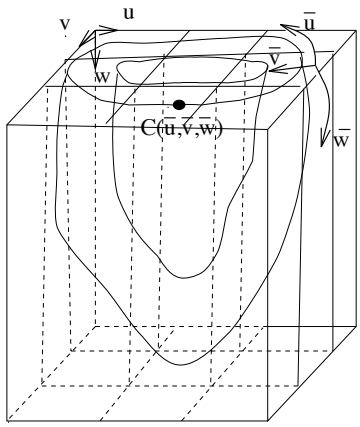

Figure 2. Coordinate systems of B-solid $(u-v-w)$ and heart model $(\overline{u}-\overline{v}-\overline{w})$ (see text)

Non-linear blending functions of the parameters $\overline{u}$ and $\overline{w}$ give a realistic shape to the heart. As for the parameter $\overline{v}$, we have used linear spline functions because our heart model is a coupled boundaries model containing information only from the epicardial and endocardial surfaces. In Fig. 3 heart contours and LV's surfaces are shown. A volumetric heart model and its LA intersection can be seen in Fig. 4.

2.3. Relation between Tag and Heart Models

In this section we show how the coordinates of points of the heart model can be expressed as functions of the parameters of the B-solid model. This will be a required step in integrating the tags and contours in the same framework. Let the point $C(\overline{u},\overline{v},\overline{w}) = (x,y,z)$ be a control point in the heart model (see Fig. 2). We need to find the parameters (u,v,w) from the B-solid so that $C = \sum_{i=0}^{I}\sum_{j=0}^{J}\sum_{k=0}^{K} S_{kji} B_i(u) B_j(v) B_k(w)$, where S_{kji} are the control vertices of the tag model.

To solve, we consider a two step procedure [14]: The first step consists of finding a linear approximation (u_0,v_0,w_0) of the parameters by solving the system,

$$C = \sum_{i=0}^{I}\sum_{j=0}^{J}\sum_{k=0}^{K} S_{kji} B_i^1(u) B_j^1(v) B_k^1(w) \qquad (1)$$

where B^1 are linear spline blending functions of the parameters and S_{kji} are the control vertices of the B-solid. The parameters (u_0,v_0,w_0) determine a point $C_0 = (x_0,y_0,z_0)$ in the cubic tag model,[1] so that: $(x_0,y_0,z_0) = \sum_{i=0}^{I}\sum_{j=0}^{J}\sum_{k=0}^{K} S_{kji} B_i(u_0) B_j(v_0) B_k(w_0)$.

[1] Here the blending functions are cubic according to the tag model

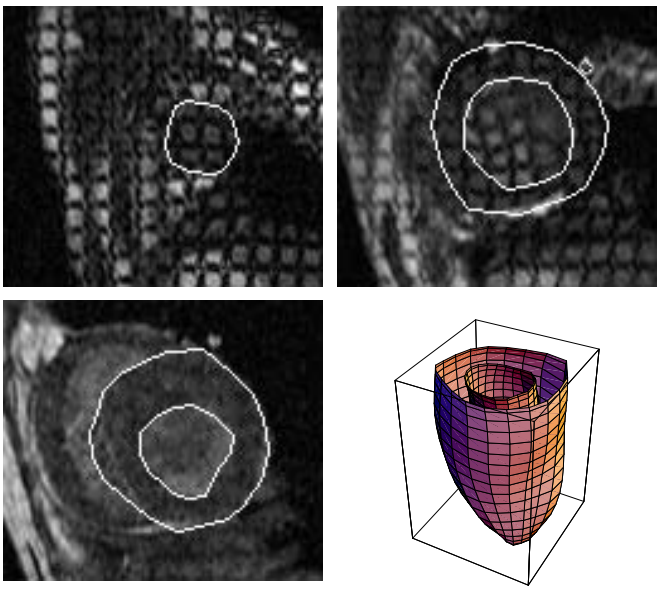

Figure 3. Heart contours and constructed endocardial and epicardial boundaries

Using a Taylor series expansion on (1) but with cubic blending functions and after simplifications, we obtain the following iterative procedure for the parameters (u, v, w),

$$
\begin{aligned}
x - x_l = {} & (u_{l+1} - u_l) \sum_{i=0}^{I} \sum_{j=0}^{J} \sum_{k=0}^{K} X_{kji} B_i'(u_l) B_j(v_l) B_k(w_l) + \\
& (v_{l+1} - v_l) \sum_{i=0}^{I} \sum_{j=0}^{J} \sum_{k=0}^{K} X_{kji} B_i(u_l) B_j'(v_l) B_k(w_l) + \\
& (w_{l+1} - w_l) \sum_{i=0}^{I} \sum_{j=0}^{J} \sum_{k=0}^{K} X_{kji} B_i(u_l) B_j(v_l) B_k'(w_l) \\
y - y_l = {} & (u_{l+1} - u_l) \sum_{i=0}^{I} \sum_{j=0}^{J} \sum_{k=0}^{K} Y_{kji} B_i'(u_l) B_j(v_l) B_k(w_l) + \\
& (v_{l+1} - v_l) \sum_{i=0}^{I} \sum_{j=0}^{J} \sum_{k=0}^{K} Y_{kji} B_i(u_l) B_j'(v_l) B_k(w_l) + \\
& (w_{l+1} - w_l) \sum_{i=0}^{I} \sum_{j=0}^{J} \sum_{k=0}^{K} Y_{kji} B_i(u_l) B_j(v_l) B_k'(w_l) \\
z - z_l = {} & (u_{l+1} - u_l) \sum_{i=0}^{I} \sum_{j=0}^{J} \sum_{k=0}^{K} Z_{kji} B_i'(u_l) B_j(v_l) B_k(w_l) + \\
& (v_{l+1} - v_l) \sum_{i=0}^{I} \sum_{j=0}^{J} \sum_{k=0}^{K} Z_{kji} B_i(u_l) B_j'(v_l) B_k(w_l) + \\
& (w_{l+1} - w_l) \sum_{i=0}^{I} \sum_{j=0}^{J} \sum_{k=0}^{K} Z_{kji} B_i(u_l) B_j(v_l) B_k'(w_l)
\end{aligned}
$$

where $l = 0, 1, \ldots$. It can be shown using the Weierstrass theorem that $\{(x_l, y_l, z_l)\}$ converges to the point (x, y, z). The procedure described here is applied to all control points of the LV model individually.

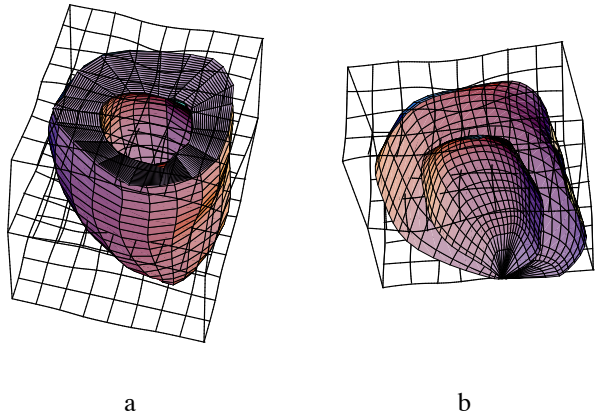

a b

Figure 4. Heart volumetric model located in a B-solid (a) and its LA (b) intersection

2.4. Tensor Product Representation of B-Solids

Considering the large amount of data in a 3D volume, the compact representation of a model and its computational complexity become of great importance. Gueziec in [5], working on the problem of surface reconstruction from 3D edge data, introduced surface representation with deformable splines by means of a 2D tensor product. There, a surface $Q(x, y, z) = \sum_{i=0}^{I} \sum_{j=0}^{J} S_{ji} B_i(u) B_j(v)$, in terms of a tensor product B-spline with $I \times J$ control points, is presented in a compact way: for all points of the surface, a matrix notation is employed: $Q = B_v^T S B_u$, where S is the control points matrix of dimensions $J \times I$, whose elements are the control vertices $S_{ji} \in R^3$. B_u (B_v) has dimensions $I \times I$ ($J \times J$) gathering all spline evaluations in the blending functions $B_i(u), i = 0, ..., I$ ($B_j(v), j = 0, ..., J$),

$$
B_u = \begin{bmatrix}
B_0(u_0) & 0 & 0 & \ldots \\
B_1(u_0) & B_1(u_1) & 0 & \ldots \\
B_2(u_0) & B_2(u_1) & B_2(u_2) & \ldots \\
B_3(u_0) & B_3(u_1) & B_3(u_2) & \ldots \\
0 & B_4(u_1) & B_4(u_2) & \ldots \\
. & . & . & .
\end{bmatrix} \qquad (2)
$$

Generalizing this notation to the solid, the control points form a 3D tensor. Using square brackets to distinguish the tensor from the matrix notation, we can write: $[Q] = [S]_{kji} \otimes_i B_u \otimes_j B_v \otimes_k B_w$, where $[Q]$ is a 3D tensor of 3-vectors representing all the sampled points of the B-solid. B_u, B_v and B_w are matrices of the form in (2), corresponding to the 3 classes of blending functions with respect to the parameters u, v and w. $[S]_{kji} =$

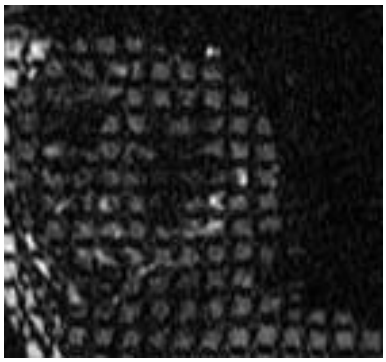

Figure 5. Original SPAMM image

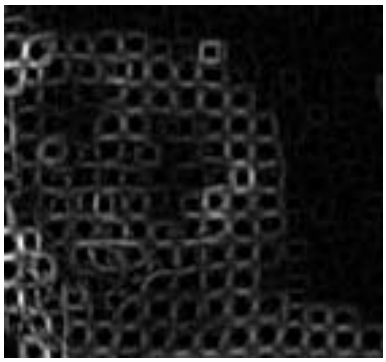

Figure 6. Map of principal curvatures

$\{S_{kji}\}_{i=0,\dots I, j=0,\dots J, k=0,\dots K}$ is a 3D tensor, whose elements are the 3-vectors of control points. In particular, the elements of $[S]_{kji}$ are ordered in such a way that fixing k and j, we obtain the control points of all u iso-parametric curves, by fixing k and i we obtain the control points of the v iso-parametric curves, etc. Each matrix of the tensor $[S_{kji}]$ formed by fixing the index k contains the control points S_{kji}, belonging to the $k-$ plane (i.e. to the w iso-parametric surface of the B-spline model), and fixing the parameters j and i we obtain the $v-$ and $u-$iso-parametric planes of the B-solid, respectively.

The operation $\otimes_l$, where l denotes an index of a tensor (e.g. $l \in \{i,j,k\}$), is defined as follows, $[S]_{kji} \otimes_i B_{im} = [\sum_{i=0}^{I} S_{kji}B_{im}]_{kjm}$, $[S]_{kji} \otimes_j B_{jm} = [\sum_{j=0}^{J} S_{kji}B_{jm}]_{kmi}$, $[S]_{kji} \otimes_k B_{km} = [\sum_{k=0}^{K} S_{kji}B_{km}]_{mji}$. The operation $\otimes_l$ is considered in more details in [14].

Because of the similarity of the multiplication $\otimes_l$ to multiplication of matrices and for sake of simplicity we shall omit the operator $\otimes_l$ accepting the following notations,

$$\begin{aligned} [S]_{kji}B_u &:= [S]_{kji} \otimes_i B_{im}(u) \\ [S]_{kji}B_v &:= [S]_{kji} \otimes_j B_{jm}(v) \\ [S]_{kji}B_w &:= [S]_{kji} \otimes_k B_{km}(w) \end{aligned}$$

3. Energy of the Deformable B-Solid

The B-solid is a deformable body with an associated energy composed of internal and external energies,

$$E_{solid} = E_{int} + E_{ext} \tag{3}$$

External forces attract the B-solid towards the tag data by minimizing its external energy E_{ext}, whereas internal forces try to preserve an ideal shape of the solid by minimizing the internal energy, E_{int}.

3.1. Tag External Energy of the Deformable B-Solid

In this paper, we propose to detect tag lines by applying a valley detector based on Haralick's facet model [7] as a more robust and invariant technique to variations in image contrast than by searching for dark regions in the image, as previously proposed. With the facet model, a pixel neighborhood is approximated by a continuous surface. All subsequent analysis is performed on the analytical representation of the facet. By observing that locations of interest in the image are dark ridges, we create a potential field whose valleys correspond to pixels with maximal principal curvature of the intensity surface, $C_{max} = \frac{1}{2}(T_{xx} + T_{yy}) + \sqrt{(T_{xx} - T_{yy})^2 + 4T_{xy}^2}$, where T denotes the surface facet (see Fig. 5 and Fig. 6).

In SPAMM-images, two sets of tag lines with approximate perpendicular orientations are present. When an implicit snake is not exactly aligned with its corresponding tag line, an attraction force from tags of perpendicular orientation acts on it which may lead the snake to settle in a wrong valley. To surmount this problem, we create two directional potential fields by filtering by a directional Gaussian the map of principal curvatures. The effect is that for the horizontal potential field, the influence of vertical features in horizontal potential field is diminished. An analogous situation holds for the vertical potential field. Thereafter, LV contours (which will be discussed later) are used to provide constant potential outside of LV myocardium. As a result implicit snakes are attracted by external forces only within the myocardium. The potential energy for each point q of an implicit snake from the deformable model Q is given by its height in the potential surface P^{tag}, $E_{ext}^{tag}(q) = P^{tag}(q),\ q \in Q$. In each step of the iterative procedure, the implicit snake is pushed by the external forces towards tag lines of same orientation.

3.2. Contour External Energy of the Heart Model

Without attempting to have any *a priori* boundary point correspondences, we consider two classes of external forces: first external force is associated with tag data, as was discussed in the last section, and the second is associated with LV boundaries.

We construct contour potentials for each image slice from successive frames using a distance map. A continuous surface with valleys corresponding to the contours is obtained by an optimization procedure described in [8]. Locating a model Q on the contour potential field, P^{cont} the potential energy of a point q is given by its height in the contour potential field $E_{ext}^{cont}(q) = P^{cont}(q),\ q \in Q$.

3.3. Internal Energy of the Deformable B-Solid

The internal energy of the classical B-snakes [11] defined in terms of derivatives up to second order preserves its continuous and smooth shape. However, minimizing the derivatives result in undesired shrinking effects. To avoid this problem, some authors minimize the difference in the membrane and thin-plate energies for the snake from an ideal model [15, 17]. In our case, we are interested in small deformations of our three dimensional solid using as a reference an ideal rectangular three dimensional model, $Q(x,y,z) = \sum_{i=0}^{I}\sum_{j=0}^{J}\sum_{k=0}^{K} S_{kji}^{0} B_u B_v B_w$. We define the internal energy as follows,

$$E_{int} = \tfrac{1}{2}\{ \sum_{r,s,t=1}^{2} \sum_{\overline{u},\overline{v},\overline{w}\in U,\ \overline{u}\neq\overline{v}\neq\overline{w}} \alpha_{\overline{u}}^{2-r}\alpha_{\overline{v}}^{2-s}\alpha_{\overline{w}}^{2-t}\beta_{\overline{u}}^{r-1}\beta_{\overline{v}}^{s-1}\beta_{\overline{w}}^{t-1} ||SB_{\overline{u}}^{(r)}B_{\overline{v}}^{(s)}B_{\overline{w}}^{(t)} - S^0 B_{\overline{u}}^{(r)}B_{\overline{v}}^{(s)}B_{\overline{w}}^{(t)}||^2 +$$
$$\sum_{r,s=1}^{2} \sum_{\overline{u},\overline{v}\in U,\ \overline{u}\neq\overline{v}} \alpha_{\overline{u}}^{2-r}\alpha_{\overline{v}}^{2-s}\beta_{\overline{u}}^{r-1}\beta_{\overline{v}}^{s-1} ||SB_{\overline{u}}^{(r)}B_{\overline{v}}^{(s)} - S^0 B_{\overline{u}}^{(r)}B_{\overline{v}}^{(s)}||^2 + \sum_{r=1}^{2}\sum_{\overline{u}\in U} \alpha_{\overline{u}}^{2-r}\beta_{\overline{u}}^{r-1} ||SB_{\overline{u}}^{(r)} - S^0 B_{\overline{u}}^{(r)}||^2 \}$$

where superscripts in parantheses denote derivatives, U is the set of parameters $\{u,v,w\}$, $B_{\overline{u}}^{(r)}, B_{\overline{u}}^{(s)}, \ldots$ are matrices formed by the $r,s,t-$derivatives of the blending functions with respect to the parameter $\overline{u}$ as shown in (2) and α and β are parameters of elasticity that determine the relative weight between the internal and external energies. Note that the notation: $\sum_{r=1}^{2}\sum_{\overline{u}\in U} \ldots B_{\overline{u}}^{(r)}$ in fact expresses all first and second derivatives of blending functions with respect to each parameter (u,v,w). In our case, we have empirically obtained that $\alpha = 0.4$ and $\beta = 10$ provide good weights for different energies. Defined in this way the internal energy of the B-solid tries to minimize the distance between the deformable body and the model.

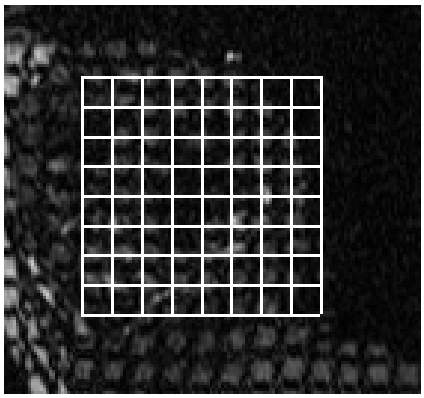

Figure 7. An intersection of the initial B-solid

4. Non-Rigid Registration of B-Solid to Tag Data

The problem of localization of tag data by a B-solid is an energy-minimizing problem. The B-solid is placed around data, and the implicit snakes are attracted by the image data. Since they determine the iso-parametric curves of the B-solid, deforming the implicit snakes deforms the solid. The local minimum of the energy that is found in image slices in the first volumetric temporal frame solves the localization problem. The resulting B-solid from each frame is then used as the initial solid in the subsequent frame in order to track the deformations.

4.1. Initialization of the B-Solid

We consider a B-solid initialization, where we do not put constraints on necessarily good approximation of the data by the implicit snakes. Instead, we consider appropriate internal forces that cope with the inexact initial positions of the deformable B-solid. The user only delimits the region of interest in one or each slices of images from the initial temporal frame and gives the initial distance between the u and v iso-parametric planes. The distance between the w-iso-parametric planes is determined by the slice separation in volumetric SA SPAMM images. The initial B-solid is defined as the minimum three-dimensional rectangular grid which contains the region(s) of interest (see Fig. 7). Since the internal force takes charge of local displacements [15], rotation and displacement of the implicit snakes between subsequent images is limited to half of the tag line interdistances.

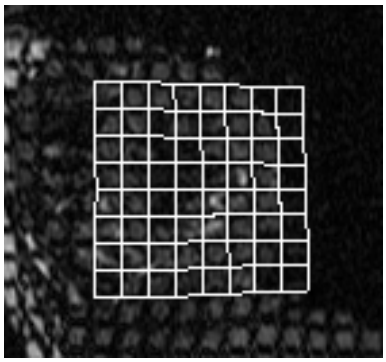

Figure 8. Tags localization by B-solid

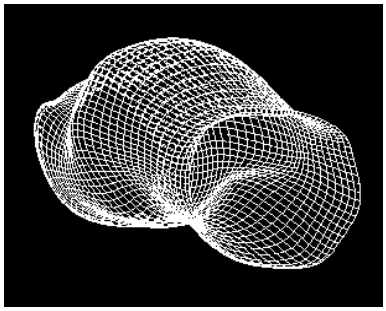

Figure 9. Endocardial B-spline approximation

4.2. Energy-Minimization Procedure

Let us consider equation (3). We are looking for a solid S that gives a minimum of the energy, E_{solid},

$$\frac{\partial E_{solid}}{\partial S} = \frac{\partial E_{int}}{\partial S} + \frac{\partial E_{ext}^{tag}}{\partial S} = 0 \tag{4}$$

A solution can be viewed as one which achieves an equilibrium between the internal and external forces in the energy equation. The solid is under the control of internal forces that impose regularity on the B-solid, whereas external forces attract the B-solid towards the data. Finding a global minimum of the considered problem is too complicated to be treatable for the B-solid. Therefore, it is important to define the external and internal forces, reflecting the need for tag localization as well as boundary tracking so that the found local minimum is a good solution for the localization problem.

To provide dynamics for the deformable body, the associated evolution equation is considered,

$$-\frac{\partial S}{\partial t} = \frac{\partial E_{int}}{\partial S} + \frac{\partial E_{ext}^{tag}}{\partial S} \tag{5}$$

A solution to the static problem (4) is achieved when the solution $S(t)$ of (5) stabilizes.

Substituting the derivatives of both energy in (5) and reducing the expression [14], we get,

$$\begin{aligned} S^{l+1} = \quad & (S^l + F_{init}(S^0) - F^{tag} B_u B_v B_w) \\ & (K_u + I)^{-1}(K_v + I)^{-1}(K_w + I)^{-1} \end{aligned} \tag{6}$$

where $K_t := \alpha_t A_t' + \beta_t A_t''$, $A_t^{(r)} := B_t^{(r)}\ B_t^{(r)T}$, t is one of $\{u, v, w\}$, $F_{init}(S^0) = S^0(K_u+I)(K_v+I)(K_w+I) - S^0$, I denotes the identity matrix and $r = 1, 2$ denotes derivative. F_{init} can be thought of as a force that always tries to push the deformable body towards the model S^0. The combination of external force and F_{init} force allows for some displacement for the deformable body and thus less dependence on initial position. In Fig. 8 a result of the localization procedure can be seen.

The linear system (6) contains three independent linear equations for (X, Y, Z) coordinates of the control vertices. Similar to the case of 1D and 2D deformable models, the three stiffness matrices regarding the three parameters $(K_u + I)$, $(K_v + I)$ and $(K_w + I)$ are diagonal, symmetric, and positive definite. Given that the parameters of elasticity are constant over time, the factorization of the matrices is done only once. This in fact, is very important for handling the 3D model fitting to the 3D data, as well as for speeding up the computational process. It is worthwhile to emphasize that in (6) the smoothing operator is presented by decoupled operators with respect to the parameters. Thus, the smoothing effect of each of them can be estimated.

5. B-Spline Approximation to Endocardium and Epicardium

The problem of localization of the LV is considered here in order to construct a LV model using the endocardial and epicardial contours in image slices in the first temporal volumetric frame. For this purpose we need approximations to endocardium and epicardium of the LV by B-spline surfaces [8]. To fit the complexity of the heart shape we have used a cubic-quadric partially closed surface with 6 slices of control points and 16 control points in each slice. We assume the heart ventricle contour points are first determined by a low-level process from tagged images or are specified on the images by the user. A potential function is defined as a distance map of the contour points and the surface model is optimized by conjugate gradient descent. This potential tolerates large deviations of the initial model to the object because even when there are some false contour points. Smoothness was enforced by applying second order derivative penalties at all points along the surface. The heart boundaries approximation allows us to construct the heart model expressed by means of the control points of the B-spline surfaces (see Fig. 9 and Fig. 10).

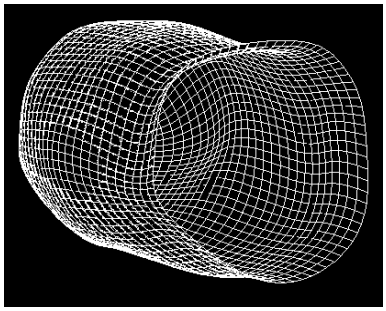

Figure 10. Epicardial B-spline approximation

6. Tracking of Heart Motion by B-Solid

The tracking procedure is analogous to the localization procedure with the only difference that tag and heart models contribute to the energy of the B-solid.

6.1. Integrated Tag Grid and Heart Boundaries Tracking

Both tag and heart models are interdependent since they are part of the same tissue. Hence, the energy minimization is done affecting only the B-solid model. The tracking problem is an energy minimizing process where the energy of the B-solid is defined by its internal, tag external and contour external energies,

$$E_{solid} = E_{int} + \omega_{tag} E_{ext}^{tag} + \omega_{cont} E_{ext}^{cont}$$

To assign equal importance to both external energies we have used equal weights $\omega_{tag} = \omega_{cont} = 1$. The contour external energy at point (x, y, z) of the solid is,

$$E_{ext}^{cont} = ||S/_H(x,y,z) - C(x,y,z)||^2 = \sum_{r=0}^{R}\sum_{s=0}^{S}\sum_{t=0}^{T} || \sum_{o=0}^{O}\sum_{p=0}^{P}\sum_{q=0}^{Q} H_{qpo} B_o(\overline{u}_r) B_p(\overline{v}_s) B_q(\overline{w}_t) - C(x,y,z)||^2$$

where H_{qpo} denotes the control vertices of number $O \times P \times Q$ of the heart boundaries and $(\overline{u}_r, \overline{v}_s, \overline{w}_t), r = 0, ..., R,\ s = 0, ..., S,\ t = 0, ..., T$ are the knots[2].

In order to find the control points S_{kji} of the B-solid associated with the control vertices H_{qpo} in the contour external energy, we apply the procedure that defines the relation between the tag and heart model given in section 2.3. Following the same energy-minimization procedure as in the tracking problem, we obtain the following iterative procedure for integrated tracking of tag and contour data,

$$S^{l+1} = (S^l + F_{init}(S^0) - F^{tag} B_u B_v B_w - F^{cont})\ (K_u + I)^{-1}(K_v + I)^{-1}(K_w + I)^{-1} \quad (7)$$

[2] Since we only have endocardial and epicardial surfaces available, $P = S = 1$ and B_p is linear.

where $F_{kji}^{cont} = 2 \sum_{o=0}^{O}\sum_{p=0}^{P}\sum_{q=0}^{Q}\sum_{r=0}^{R}\sum_{s=0}^{S}\sum_{t=0}^{T} B_o(\overline{u}_r)\ B_p(\overline{v}_s)\ B_q(\overline{w}_t) B_i(u_0) B_j(v_0) B_k(w_0)$.

In Fig. 11 and Fig. 12 an example of two frames considered in the tracking process is shown. At the base of the heart the grid is not deformed because the external force is applied only to the heart tissue. In Fig. 12 (c) and (d) a slice of the tracked heart located in the B-solid can be seen.

Note that no correspondence of points between nodes of the model and tag intersections is necessary. In addition, the interpolation of forces to nodes of the model is implicit.

6.2. Numerical Complexity

In the usual way of treating high-dimensional deformable models problem [17], the data are presented in a vector and the resulting linear systems (6) and (7) will be of size $((IJK) \times (IJK))$. In addition, the matrices are sparse but not diagonal [17, 18]. In the case of B-solid from (6) and (7), it can be seen that the numerical complexity of each iteration of the energy-mimizing procedure is $O(I \times J \times K)$ and the 3 stiffness matrices are diagonal. This fact is very important so as to make the procedure practical and in dealing with real 3D image analysis problems. The B-solid algorithm is implemented in C on a SUN Sparc station and takes about 6 minutes for each temporal frame to localize or track a B-solid with 600 control points.

7. Extension of the Approach to the Analysis of SA and LA Images

In case of SA images since the external forces of the implicit snakes belong to the imaging planes, the deformation of the B-solid caused by the tag and contour data is mainly in the plane $(x-y)$. The internal forces are three-dimensional yet this is not sufficient to provide out-of-plane movement of the material points of the heart. To solve this problem, authors have combined images of short and long axes views.

Here we describe how to obtain three-dimensional tissue movement by treating SA images with two-dimensional tags and LA images with one-dimensional tags; i.e., we assume that in the SA views there are two sets of perpendicular tag planes, whereas in the LA images there is only one set of horizontal tag planes. Let us consider SA view images where the imaging planes are parallel to the $(x-y)$ plane. From the fact that tagging planes are orthogonal to the imaging planes, it follows that the tagging planes are parallel to the planes $(x-z)$ and $(y-z)$ initially. Without loss of generality, we can consider that in the LA view the imaging planes are parallel to the plane $(x-z)$ and the tagging planes are parallel to the planes $(x-y)$ (see Fig. 13 and 14). Since a main source of information about the tissue movement is given by the deformation of the tag planes, we define the B-solid so that the

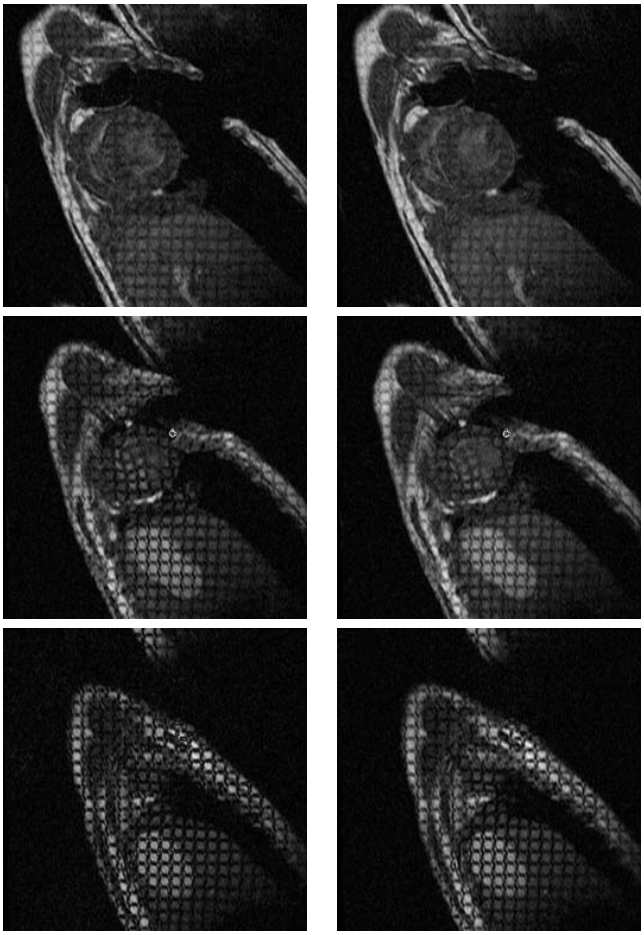

Figure 11. Tracking of deformation: different slices of images from two consecutive frames given in the first and second column

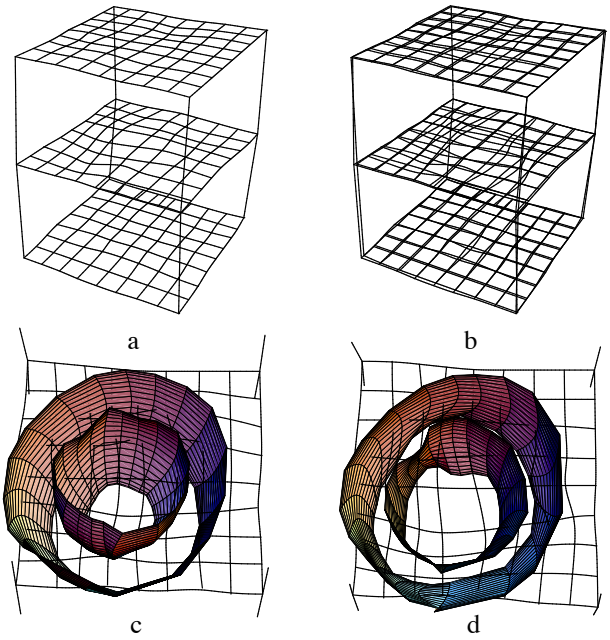

Figure 12. B-solids from first (a) and two consequetive frames (b) and slices of heart boundaries from both temporal frames (c) and (d).

iso-parametric planes correspond to the tagging planes. In particular, u and v iso-parametric planes are aligned with tag planes from the SA images and w iso-parametric planes are aligned with the tag planes from the LA images.

By definition the external forces of the B-solid are applied to the control vertices. The external forces of the B-solid are obtained by running patches on the iso-parametric curve and assigning the overall external force to the control vertices. In the case of B-solids constructed by SA view images, the u and v iso-parametric curves belong to the imaging planes. Since the potential field is constructed by considering the features (principal curvatures) of the imaging planes, the external forces are defined for each point of the imaging plane, in particular for the points of the iso-parametric curves.

In case of B-solid constructed by SA and LA view images, the iso-parametric curves do not belong to the imaging planes. The iso-parametric curves (e.g. the curve SP in Fig. 13) intersect the imaging planes in tag lines (e.g. curves PU and PV). We estimate the external force on the control points considering the tag lines analogous to the case of implicit snakes in B-solid constructed from SA images [14]. Once we have determined the external forces on the implicit snakes, we apply the energy-minimization procedure to localize the tag and contour data and track the heart motion.

8. Conclusions

In conclusion, a novel three-dimensional B-solid deformable model is proposed for locating, and tracking the LV deformations in a time sequence of 3D volumetric SPAMM images with implicit snakes. B-spline bases provide local control of shape, compact representation, and parametric smoothness. The B-solid proposed in the paper deforms in space, adjusting to tag and contour data from different slices reflecting the natural continuity and smoothness of the three-dimensional tissue deformations. As a consequence of the approach, localization, displacement fitting and interpolation of tag and contour information are performed in a single procedure making use of B-spline bases. A LV volumetric model was also constructed to incorporate data from endocardial and epicardial boundaries and restricts the image

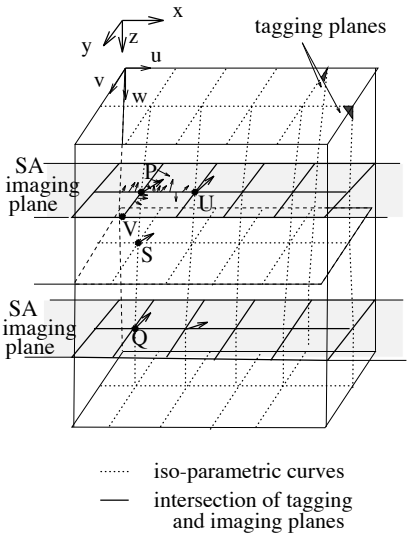

Figure 13. B-solid intersection with a SA image

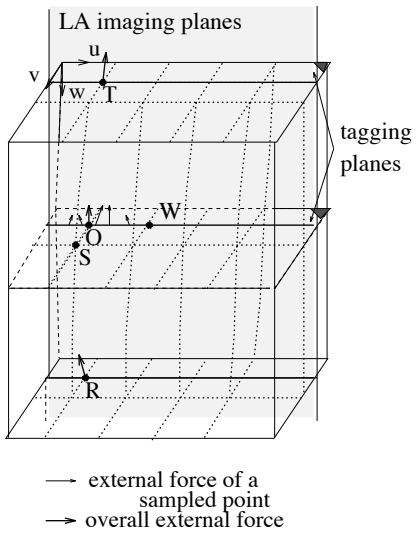

Figure 14. B-solid intersection with a LA image

forces to the heart tissue.

In applying the B-solid to tagged images, information from data in different slices are used, making the approach robust and precise against noise. Although the deformable B-solid presented here was created from tensor product of non-periodic B-splines in the cartesian coordinate frame, it is also possible to create B-solids adaptable to analysis of star-burst tagged MR images.

The B-solid defined here detects local heart's deformations. Our future work includes extraction of 3D motion of LV's material points with B-solids as discussed in section 7.

Acknowledgements

This work has been supported by a grant TIC91-0430 from MEC of Spain and grants from NSF and The Whitaker Biomedical Engineering Foundation.

References

[1] A. Amini. *Energy Minimizing Deformable Grids for Tracking Tagged MR Cardiac Images*. Proc. of CiC, 1992.

[2] A. Amini, R. Curwen, and J. Gore. *Snakes and Splines for Tracking Non-Rigid Heart Motion*. ECCV, UK, 1996.

[3] L. Axel and L. Dougherty. MR imaging of motion with spatial modulation of magnetization. *Radiology*, 171(3), 1989.

[4] R. Bartels, J. Beatty, and B. Barsky. *An Introduction to Splines for Use in Computer Graphics and Image Modelling*. Morgan Kauffmann, 1987.

[5] A. Gueziec. Surface representation with deformable splines: Using decoupled variables. *IEEE Comp. Sci. and Engineering*, 1995.

[6] M. A. Guttman, J. L. Prince, and E. R. McVeigh. Tag and contour detection in tagged MR images of the left ventricle. *Trans. on Med. Imaging*, 1994.

[7] R. M. Haralick and L. G. Shapiro. *The Facet Model*. Computer and Robot Vision, Addison-Wesley, 1992.

[8] J. Huang and A. Amini. *Deformable B-Spline Surfaces for Localization of Tubular Structures in 3D Medical Images*. Tech. Report, Yale University, New Haven, USA, 1996.

[9] D. L. Kraitchman, A. A. Young, C.-N. Chang, and L. Axel. Semi-automatic tracking of myocardial motion in mr tagged images. *IEEE Trans. Med. Imaging*, 14(3):422–433, 1995.

[10] S. Kumar and D. Goldgof. Automatic tracking of spamm grid and the estimation of deformation parameters from cardiac mr images. *IEEE Trans. Med. Imaging*, 13(1), 1994.

[11] S. Menet, P. Saint-Marc, and G. Medioni. *B-Snakes: Implementation and Application to Stereo*. Proc. DARPA Image Understanding Workshop, Pittsburgh, 1990.

[12] W. G. O'Dell, C. C. Moore, W. C. Hunter, E. A. Zerhouni, and E. R. McVeigh. Three-dimensional myocardial deformations: Calculation with displacement field fitting to tagged MR images. *Radiology*, 195, 1995.

[13] J. Park, D. Metaxas, and L. Axel. *Volumetric Deformable Models with Parameter Functions: A New Approach to the 3D Motion Analysis of the LV from MRI-SPAMM*. Proc. of ICCV, MIT, 1995.

[14] P. Radeva, A. Amini, J. Huang, and E. Martí. *Deformable B-Solid: Application to Tracking of MRI-SPAMM Data*. Tech. Report, UPIIA, UAB, 1996.

[15] P. Radeva, J. Serrat, and E. Martí. *A Snake for Model-Based Segmentation*. Proc. of ICCV, Cambridge, 1995.

[16] K. R. Symon. *Mecanica*. Aguilar, Madrid, 1970.

[17] D. Terzopoulos, J. Platt, A. Barr, and K. Fleisher. Elastically deformable models. *Computer Graphics*, 21(4), 1987.

[18] A. A. Young, D. L. Kraitchman, L. Dougherty, and L. Axel. Tracking and finite element analysis of stripe deformation in magnetic resonance tagging. *IEEE Trans. on Med. Imaging*, 14(3):413–421, 1995.